LBL-11498
GREMP-12
UC-66a

A Theoretical Assessment of James' Method for the Determination of Geothermal Wellbore Discharge Characteristics

Madhav Karamarakar and Ping Cheng

November 1980

Geothermal Reservoir Engineering Management Program

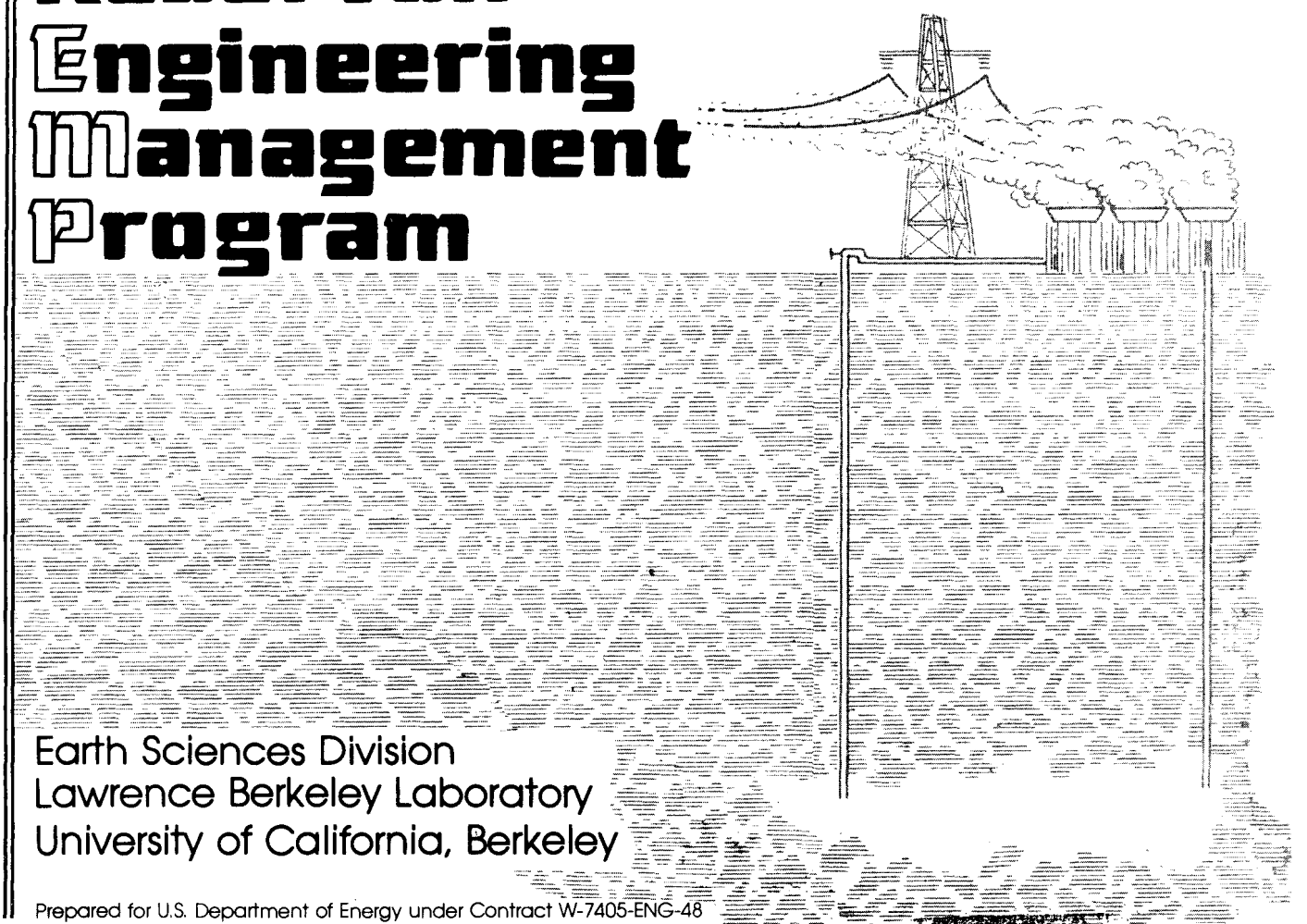

Earth Sciences Division
Lawrence Berkeley Laboratory
University of California, Berkeley

Prepared for U.S. Department of Energy under Contract W-7405-ENG-48

LBL-11498

GREMP-12

A THEORETICAL ASSESSMENT OF JAMES' METHOD FOR THE DETERMINATION OF GEOTHERMAL WELLBORE DISCHARGE CHARACTERISTICS

Madhav Karamarakar and Ping Cheng

Department of Mechanical Engineering
University of Hawaii at Manoa
Honolulu, Hawaii 96722

November 1980

This report was prepared by the University of Hawaii at Manoa, Honolulu, Hawaii under Lawrence Berkeley Laboratory Purchase Order No. 4501510. The subject research is pursuant to the LBL contract with the U. S. Department of Energy, Division of Geothermal Energy for Geothermal Reservoir Engineering Research. It was administered under the technical direction of C. W. Miller, A. N. Graf, J. H. Howard, and W. Schwarz. Mr. Rich Arriaga was the Contract Administrator for LBL, under contract W-7405-ENG-48.

TABLE OF CONTENTS

INTRODUCTION 1

1.1 Background. 1
1.2 Objectives. 1

APPLICATIONS OF ONE-COMPONENT TWO-PHASE CRITICAL FLOW MODELS. 1

2.1 Background. 1
2.2 Fauske's Model 2
2.3 Moody's Model 3
2.4 Levy's Model 4
2.5 Results and Discussion 5

THE EFFECT OF NON-CONDENSIBLE GASES ON THE WELLBORE

DISCHARGE CHARACTERISTICS. 6

3.1 Background. 6
3.2 The Extension of Fauske's Model 6
3.3 Results and Discussion 8

THE EFFECT OF DISSOLVED SOLIDS ON THE WELLBORE

DISCHARGE CHARACTERISTICS 8

4.1 Background. 8
4.2 An Extension of Fauske's Model. 8
4.3 Results and Discussion 8

THE EFFECTS OF LIP PRESSURE TAPPING POSITION AND

PIPE DIAMETER 10

5.1 Background. 10
5.2 Analysis of Pressure Drop Behavior 10
5.3 Results and Discussion 11

CONCLUDING REMARKS 11

REFERENCES. 11

A THEORETICAL ASSESSMENT OF JAMES' METHOD FOR THE DETERMINATION OF GEOTHERMAL WELLBORE DISCHARGE CHARACTERISTICS

ACKNOWLEDGMENTS

This work was performed under purchase order #4501510 for the Lawrence Berkeley Laboratory, University of California, Berkeley, California, as part of the Geothermal Reservoir Engineering Management Program, sponsored by the United States Department of Energy, Division of Geothermal Energy.

The authors would like to thank A. Graf and C.W. Miller for the critical reading of the manuscript.

INTRODUCTION

1.1 Background

Geothermal resources can be classified as hydrothermal convective (i.e., hot-water, two-phase, or dry-steam), geopressured, hot rock, or magma systems [1]. With the present technology, only the hydrothermal convective systems are economically viable for power generation. To estimate the power production of a geothermal well during field development and exploitation, it is important to know the wellhead discharge characteristics such as the flow rate, stagnation enthalpy, and steam quality. If a single-phase flow (hot-water or dry steam) exists at the wellhead, its flow rate can be measured accurately by means of an orifice. It is known, however, that using the same device for the measurements of two-phase flow may lead to serious errors [2].

One of the most simple and accurate methods for the determination of flashing geothermal wellbore discharge characteristics is the so-called James' method [3,4]. The method is based on the observation that the flashing geothermal fluid discharging from the wellhead usually attain sonic speeds at the exit because of the lower pressure at the exit cross section. Figure 1 shows a typical set up on a geothermal well site for determining the discharge characteristics based on the James' method [5]. The flashing geothermal fluid from the wellhead is discharged through a horizontal tube into the twin-tower stacks where steam and liquid-water are separated. If the static pressure (p) at the exit of the horizontal tube (where the discharge fluid attains sonic speeds at the exit) and the liquid-water flow rate (w) discharges from the stacks (as measured by a conventional weir) are measured, the stagnation enthalpy (h_o) can then be determined from a plot of h_o versus $w/p^{0.96}$ as shown in Fig. 2 where h_o is in Btu/lb_m, w in lb_m/sec-ft^2, and p in psia. The data presented in Fig. 2 was empirically determined by James. The total mass flow rate is determined from the following empirical formula

$$G_M = 11{,}400\ p^{0.96}/h_o^{1.102}\ , \qquad (1.1)$$

where G_M is the total mass flow rate per unit area in lb_m/sec-ft^2, p is the lip pressure and h_o is the stagnation enthalpy. Equation (1.1) was empirically determined by James [3,4] for steam-liquid water mixtures with discharge pressures up to 64 psia and for pipe diameters of 3", 6", and 8" with stagnation enthalpy ranging from 270 Btu/lb_m to 1,200 Btu/lb_m.

The exit steam quality can then be determined by using the following equation

$$x = (G_M - w)/G_M\ . \qquad (1.2)$$

It should be noted that Eq. (1.1) is not valid if the discharged fluid contains a substantial amount of dissolved solids and/or other non-condensible gases, both of which may be present in geothermal wellbores.

1.2 Objectives

The objectives of this study are:

1. To evaluate the accuracy of James' method for the determination of flow rate, stagnation enthalpy and steam quality in the wellbore by comparing results based on the one-component two-phase critical models by Fauske [6,7], Moody [8] and Levy [9,10].
2. To investigate the effects of non-condensible gases and dissolved solids on the wellbore discharge characteristics by extending the one-component two-phase critical flow methods to include these extra components.
3. To determine the effects of lip pressure tapping position and pipe diameters on the accuracy of lip pressure measurements, by studying theoretically, the pressure gradients in the approach region to the critical flow.

APPLICATIONS OF ONE-COMPONENT TWO-PHASE CRITICAL FLOW MODELS

2.1 Background

It is well known that if the velocity of the two-phase flow is high enough [6], an annular or separated flow pattern will be established in the pipe (see Fig. 3). Such is usually the case for the two-phase flow in the horizontal discharge pipe in Fig. 1. In this chapter, the two-phase one-component critical flow models developed by Fauske [6,7], Moody [8], and Levy [9,10] will be briefly reviewed, the methods of computing the critical flow rate, stagnation enthalpy, and steam quality based on these models will be discussed, and the results will be presented in an easy-to-use form suitable for geothermal well testing purposes. Finally, a comparison of results based on James' method and those predicted by theoretical models will also be made.

The common assumptions employed in these one-component two-phase critical models are:

1. An annular flow pattern is assumed. Each phase is represented by "lump" nature and assumed to be flowing with a single mean velocity in the direction of the flow (see Fig. 4).
2. Velocity slip occurs between the two phases.
3. The flow is adiabatic and one-dimensional.
4. Static pressure at any cross section is the same for both phases and is uniform along the cross section.
5. Both phases are assumed in local equilibrium with each other. This assumption is supported by several experimental studies on the duration of non-equilibrium states [10]. As a result the analysis is considerably simplified because considerations for interfacial heat and mass transfer are not necessary.
6. The flow is steady. The implications of this assumption was discussed by Moody [11] who shows that this assumption together with the critical flow condition, $dG/dp = 0$ (where G is the mass flow rate per unit area and p is the static pressure) would lead to the satisfaction of sonic flow at the critical conditions.

With these assumptions, the continuity equations for the vapor and liquid phases are

$$\dot{m}_g = xGA \ , \tag{2.1a}$$

$$\dot{m}_f = (1 - x)GA \ , \tag{2.1b}$$

where $\dot{m}_g$ and $\dot{m}_f$ are the mass flow rate of vapor and liquid respectively, x is the steam quality, A the cross sectional area, and G the total mass flow rate per unit area. It follows from Eq. (2.1) that the velocity of the vapor phase (u_g) and that of the liquid phase (u_f) are given by

$$u_g = Gxv_g/\alpha \ , \tag{2.2a}$$

$$u_f = G(1 - x)v_f/(1 - \alpha) \ , \tag{2.2b}$$

where v_g and v_f are the specific volume of the vapor and the liquid, and α is the void fraction defined as $\alpha = A_g/A$ and consequently $1 - \alpha = A_f/A$, with A_g and A_f denoting the areas occupying by the vapor and liquid water respectively. Elimination of G between Eq. (2.2a) and Eq. (2.2b), gives

$$\alpha = \frac{1}{1 + \frac{k(1-x)}{x}\frac{v_f}{v_g}} \ , \tag{2.3}$$

where k is the slip ratio defined as

$$k = u_g/u_f \ . \tag{2.4}$$

The momentum equation for the liquid phase is

$$-A_f dp - dF_f - \frac{d(\dot{m}_f u_f)}{g_c} + \frac{u_f d\dot{m}_f}{g_c} = 0 \ , \tag{2.5a}$$

while that of the vapor phase is

$$-A_g dp - dF_g - \frac{d(\dot{m}_g u_g)}{g_c} + u_f \frac{d\dot{m}_g}{g_c} = 0 \ , \tag{2.5b}$$

where $g_c \equiv 32.2$ lb_m-ft/lb_f-sec^2 (for the British Engineering system), dF_f and dF_g are the frictional force applied to the liquid and vapor phases respectively. Adding Eqs. (2.5a) and (2.5b) and noting that $d\dot{m}_f = -d\dot{m}_g$, we have the following momentum equation for the mixture

$$-Adp - \frac{1}{g_c} d(\dot{m}_f u_f + \dot{m}_g u_g) - dF = 0 \ , \tag{2.5c}$$

where $dF = dF_f + dF_g = (fG^2Av/2g_cD)dz$ is the total frictional force over dz, with v denoting some specific volume for the mixture, D the diameter of the pipe and f the friction coefficient.

The energy equation for the adiabatic one-dimensional annular two-phase flow is

$$h_o = x\left[h_g + \frac{u_g^2}{2g_cJ}\right] + (1 - x)\left(h_f + \frac{u_f^2}{2g_cJ}\right) \ , \tag{2.6a}$$

where h_o is the stagnation enthalpy, h_f and h_g are the enthalpy of the liquid and water vapor and J is the conversion factor (J = 778 ft-lb_m/Btu). With the aid of Eqs. (2.2), the above equation can be rewritten as

$$h_o = [h_f(1-x) + h_g x] + \frac{G^2}{2g_cJ}[E], \tag{2.6b}$$

$$\text{where } E = \left[\frac{x^3 v_g^2}{\alpha^2} + \frac{(1 - x)^3 v_f^2}{(1 - \alpha)^2}\right]. \tag{2.6b}$$

Equations (2.1)-(2.6) are the governing equations for one-component two-phase flow based on the annular flow pattern.

2.2 Fauske's Model

The first step in Fauske's analysis [6,7] is the identification of the specific volume v in the annular two-phase flow. This can be achieved by substituting Eqs. (2.1) and (2.2) into Eq. (2.5c) to given

$$\frac{G^2}{g_c}\left\{d\left[\frac{x^2 v_g}{\alpha} + \frac{(1-x)^2 v_f}{1-\alpha}\right] + \frac{fvdz}{2D}\right\} + dp = 0 \tag{2.7a}$$

Fauske compared Eq. (2.7a) with the single-phase equation

$$\frac{G^2}{g_c}\left[dv' + \frac{fv'dz}{2D}\right] + dp = 0 \ , \tag{2.7b}$$

and noted that these equations are identical in form if the specific volume v for the two-phase flow is defined as

$$v = \frac{(1-x)^2 v_f}{(1-\alpha)} + \frac{x^2 v_g}{\alpha} \quad . \tag{2.8}$$

Substituting Eq. (2.8) into Eq. (2.7a), it can be shown that the pressure gradient at a given location is a function of G, x, and k. For the annular two-phase flow, Fauske [6] proposed that at the critical flow condition the absolute value of the pressure gradient at a given location is maximum and finite for a given flow rate and quality, i.e.,

$$\left(\frac{dp}{dz}\right)_{G,x} = \text{maximum and finite} \quad . \tag{2.9}$$

It follows from Eq. (2.9) that the critical condition occurs if

$$\frac{\partial}{\partial k}\left(\frac{dp}{dz}\right)_{G,x} = 0 \quad . \tag{2.10}$$

Substituting Eq. (2.8) into Eq. (2.7a) and performing the differentiation with respect to k as indicated by Eq. (2.10) leads to

$$\frac{G^2}{g_c}\left[\frac{d}{dz}\left(\frac{\partial v}{\partial k}\right) + \frac{f}{2D}\left(\frac{\partial v}{\partial k}\right) + \frac{v}{2D}\left(\frac{\partial f}{\partial k}\right)\right] = 0 \quad , \tag{2.11}$$

which implies

$$\left(\frac{\partial v}{\partial k}\right) = 0 \quad , \tag{2.12a}$$

$$\left(\frac{\partial f}{\partial k}\right) = 0 \quad , \tag{2.12b}$$

Equation (2.12b) was experimentally verified by Fauske [5] with the interpretation that f goes through a maximum at the critical flow cross section. Equations (2.12a) and (2.8) lead to the following expression for k at the critical flow cross section

$$k_M = \sqrt{\frac{v_g}{v_f}} \quad . \tag{2.13}$$

Substituting Eq. (2.13) into Eq. (2.3), Fauske obtains the following expression for void fraction at the critical flow cross section

$$\alpha_M = \frac{1}{\left[1 + \frac{1-x}{x}\left(\frac{v_g}{v_f}\right)^{1/2}\right]} \quad . \tag{2.14}$$

Integrating Eq. (2.7a) between P_o and P, differentiating the resulting equation with respect to p, and then imposing the critical flow condition $dG/dp = 0$, Fauske obtains the following expression for the critical flow rate

$$G_M = \left[\frac{-g_c k_M}{\frac{dv_g}{dp}\left[(1-x+k_M x)x\right] + \frac{dx}{dp}\left\{v_g(1+2k_M x-2x) + v_f k_M\left[2x(1-k_M) + (k_M-2)\right]\right\}}\right]^{1/2} \quad . \tag{2.15}$$

In arriving at the expression given by Eq. (2.15), the term dv_f/dp has been neglected in comparison with the term dv_g/dp which is valid for pressures up to 400 psia. To evaluate the term dx/dp in Eq. (2.15), Fauske [5] assumed that the flow is at constant enthalpy, i.e., dh = 0 where

$$h = h_f + x h_{fg} \quad . \tag{2.16a}$$

Differentiating Eq. (2.16a) with respect to p and noting dh = 0, we have

$$\frac{dx}{dp} = -\frac{1}{h_{fg}}\left(\frac{dh_f}{dp} + x\frac{dh_{fg}}{dp}\right) \quad . \tag{2.16b}$$

Thus, for given values of lip pressure and steam quality, Eq. (2.15) together with Eq. (2.16b) can be used to compute the critical flow rate with the aid of a steam table. After the critical flow rate has been obtained, the weir flow rate can be computed according to Eq. (2.1b) which gives

$$w = \dot{m}_f/A = (1-x)G_M \quad , \tag{2.17}$$

while the stagnation enthalpy can be computed according to Eq. (2.6b) with the aid of Eq. (2.14). Computations for the critical mass flow rate, weir flow rate, and stagnation enthalpy were carried out for lip pressure in the range of 14.7 psia to 150 psia with saturated properties given by a steam table [12]. Results are presented in Figs. 5 and 6.

For geothermal well tests, the weir flow rate and lip pressure can be measured. Thus, steam quality and stagnation enthalpy can be determined from Figs. 5 and 6. The total mass flow rate can be computed according to

$$G_M = \frac{w}{(1-x)} \quad . \tag{2.18}$$

2.3 Moody's Model

Using the continuity equations (2.1a), the energy equation, Eq. (2.6a), and with the aid of Eq. (2.4), Moody [8] obtains the following expression for the mass flow rate per unit area

$$G = \left\{\frac{2g_c J[h_o - xh_{fg} - (1-x)h_f]}{[xv_g + (1-x)kv_f]^2\left(x + \frac{1-x}{k}\right)}\right\}^{1/2} \quad . \tag{2.19}$$

If an isentropic process is assumed, then

$$s_o = s = s_f + x s_{fg} \quad , \tag{2.20}$$

from which $x = \frac{s_o - s_f}{s_{fg}}$ and $1-x = \frac{s_g - s_o}{s_{fg}}$.

Substitution of Eq. (2.20) into Eq. (2.19), Moody [8] obtains

$$G = \left\{ \frac{2g_c J\left[h_o - h_f - \frac{h_{fg}}{s_{fg}}(s_o - s_f)\right]}{[A]^2[B]} \right\}^{1/2} , \quad (2.21)$$

where $A = \frac{k(s_g - s_o)v_f}{s_{fg}} + \frac{(s_o - s_f)v_g}{s_{fg}}$,

$$B = \frac{s_o - s_f}{s_{fg}} + \frac{s_g - s_o}{k^2 s_{fg}} ,$$

which clearly shows that G is a function of k and p when h_o and s_o are known. It follows that G is a maximum when

$$\left(\frac{\partial G}{\partial k}\right)_p = 0 , \quad (2.22a)$$

$$\left(\frac{\partial G}{\partial p}\right)_k = 0 . \quad (2.22b)$$

Imposing condition (2.22a) on Eq. (2.21) leads to

$$k_M = \left(\frac{v_g}{v_f}\right)^{1/3} , \quad (2.23)$$

which shows that k depends only on p at the maximum flow rate. Equations (2.21) and (2.22) with the well known thermodynamic relationships lead to the following expression for the maximum flow rate per unit area in terms of the local properties

$$G_M = \sqrt{2g_c \frac{J}{J'} \frac{c}{a(ad + 2be)}} , \quad (2.24a)$$

with

$$\begin{aligned}
a &= k_M v_{fM} + x_M(v_{gM} - k_M v_{fM}) , \\
b &= 1/k_M^2 + x_M(1 - 1/k_M^2) , \\
c &= -(v_{fM} + x_M v_{fgM}) , \\
d &= \left[\frac{s_g'}{k^2 s_{fg}} - \frac{s_f'}{s_{fg}} - \frac{(s_{fg}k^2)'}{k^4 s_{fg}}\right]_M + x_M\left[\frac{(s_{fg}k^2)'}{k^4 s_{fg}} - \frac{s_{fg}'}{s_{fg}}\right]_M , \\
e &= \left[s_{fg}\left(\frac{kv_f}{s_{fg}}\right)' + \left(\frac{kv_f}{s_{fg}}\right)s_g' - \left(\frac{v_g}{s_{fg}}\right)s_f'\right]_M + x_M\left[s_{fg}\left(\frac{v_g}{s_{fg}}\right)' - s_{fg}\left(\frac{kv_f}{s_{fg}}\right)'\right]_M ,
\end{aligned} \quad (2.24b)$$

where k_M is determined from Eq. (2.23), J'=J/144 and primes denote derivatives with respect to p. With G_M thus obtained, the stagnation enthalpy was obtained by substituting G_M into Eq. (2.21) and the weir flow rate is obtained from Eq. (2.18). The results of the computations for lip pressure from 14.7 to 150 psia are presented in Figs. 7-8.

2.4 Levy's Model

Levy [9,10] assumed that frictional force is negligible in his analysis. The substitution of the continuity equations (2.2) into the momentum equation for the mixture, Eq. (2.5c) with the frictional force neglected, leads to

$$G = \left[-g_c/\left(\frac{dv}{dp}\right)\right]^{1/2} , \quad (2.25)$$

where v is given by Eq. (2.8). The above equation for G will be maximum when the process is isentropic, i.e.,

$$G_M = \left[-g_c/\left(\frac{dv}{dp}\right)_s\right]^{1/2} . \quad (2.26)$$

To evaluate $\left(\frac{dv}{dp}\right)_s$, Levy [9] noted that

$$v = v(p,x) , \quad (2.27a)$$

$$dv = \left(\frac{\partial v}{\partial p}\right)_x dp + \left(\frac{\partial v}{\partial x}\right)_p dx , \quad (2.27b)$$

so that

$$\left(\frac{dv}{dp}\right)_s = \left(\frac{\partial v}{\partial p}\right)_x + \left(\frac{\partial v}{\partial x}\right)_p \left(\frac{dx}{dp}\right)_s . \quad (2.27c)$$

To obtain the partial derivatives $\left(\frac{\partial v}{\partial p}\right)_x$ and $\left(\frac{\partial v}{\partial x}\right)_p$, Levy used the relationship between x and α which he obtained as follows. Dividing Eqs. (2.5a) and (2.5b) by A_f and A_g respectively and subtracting the resulting equations from each other yields

$$d[\rho_g A_g u_g^2 + \rho_f u_f^2] - A\rho_f u_f du_f = 0 . \quad (2.28)$$

With the aid of Eqs. (2.2), Eq. (2.28) can be rewritten as

$$\frac{d}{dx}\left[\frac{(1-x)^2}{(1-\alpha)} + \frac{x^2}{\alpha}\frac{\rho_f}{\rho_g} - \frac{1}{2}\frac{(1-x)^2}{(1-\alpha)^2}\right] = 0 , \quad (2.29)$$

which can be integrated to give

$$\frac{(1-x)^2}{(1-\alpha)} + \frac{x^2}{\alpha}\frac{\rho_f}{\rho_g} - \frac{1}{2}\frac{(1-x)^2}{(1-\alpha)^2} = 0 , \quad (2.30)$$

where the condition that $\alpha = 0$ at $x = 0$ has been imposed. From Eq. (2.30), Levy [10] obtained a relation between α and x as

$$x = \frac{\alpha(1-2\alpha) + \alpha\sqrt{(1-2\alpha)^2 + \alpha\left[2\left(\frac{v_g}{v_f}\right)(1-\alpha)^2 + \alpha(1-2\alpha)\right]}}{\left(2\frac{v_g}{v_f}\right)(1-\alpha)^2 + \alpha(1-2\alpha)} \quad . \tag{2.31}$$

The partial derivatives $\left(\frac{dv}{dp}\right)_x$ and $\left(\frac{\partial v}{\partial x}\right)_p$ in Eq. (2.27c) can now be obtained by differentiating Eqs. (2.8) and 2.31) to give

$$\left(\frac{\partial v}{\partial x}\right)_p = \frac{\left[v_f(1-x)^2\right]\left[\frac{2(1-x)v_f}{(1-\alpha)} - \frac{2xv_f}{\alpha} - \frac{(1-x)v_f}{(1-\alpha)^2}\right]}{(1-\alpha)^3\left[v_f\frac{(1-x)^2}{(1-\alpha)^2} - \frac{x^2v_g}{\alpha^2} - v_f\frac{(1-x)^2}{(1-\alpha)^3}\right]} - \frac{v_f(1-x)}{(1-\alpha)^2} , \tag{2.32}$$

$$\left(\frac{\partial v}{\partial p}\right)_x = \frac{\left[v_f\frac{(1-x)^2x^2}{\alpha}\right]\left[\frac{v_g}{v_f}\left(\frac{dv_f}{dp}\right) - \left(\frac{dv_g}{dp}\right)\right]}{(1-\alpha)^3\left[v_f\frac{(1-x)^2}{(1-\alpha)^2} - \frac{x^2v_g}{\alpha^2} - v_f\frac{(1-x)^2}{(1-\alpha)^3}\right]} + \frac{1}{2}\left(\frac{dv_f}{dp}\right)\left[1 + \frac{(1-x)^2}{(1-\alpha)^2}\right] . \tag{2.33}$$

Finally, the partial derivative $\left(\frac{dx}{dp}\right)_s$ in Eq. (2.27c) can be obtained as follows. Since

$$s = s(x,p) = s_f(1-x) + x\,s_g , \tag{2.34}$$

and for an isentropic process

$$ds = \left(\frac{\partial s}{\partial p}\right)_x dp + \left(\frac{\partial s}{\partial x}\right)_p dx = 0 , \tag{2.35}$$

so that

$$\left(\frac{dx}{dp}\right)_s = -\frac{\left(\frac{\partial s}{\partial p}\right)_x}{\left(\frac{\partial s}{\partial x}\right)_p} = -\frac{(1-x)\left(\frac{ds_f}{dp}\right) + x\left(\frac{ds_g}{dp}\right)}{s_g - s_f} . \tag{2.36}$$

Thus, for given values of p and α, the steam quality can be computed according to Eq. (2.31) while the mass flow rate can be computed according to Eq. (2.26), together with Eqs. (2.27c), (2.32), (2.33) and (2.36) and with steam properties given by a steam table [12]. Computations were carried out for lip pressures from 14.7 to 150 psia and the results are plotted in Figures 9 and 10.

2.5 Results and Discussion

The three theoretical models for the computations of critical mass flow rate differ from one another in essentially three aspects: (i) assumptions employed, (ii) governing equations used, and (iii) the criterion for two-phase critical flow to occur. The last assumption leads to different expressions for slip ratio at the critical condition.

Using the continuity and momentum equations, Fauske [6] proposed that at the critical flow condition the pressure gradient is maximum and finite for a given flow rate and quality. The criterion is given by Eq. (2.9) which led to the slip ratio given by Eq. (2.13). On the other hand, Moody [8] used the continuity and energy equations and assumed that the slip ratio at the exit to be an independent variable to maximize the flow rate with respect to both k and p. This criterion is given in Eq. (2.22) which led to the slip ratio given by Eq. (2.23).

Levy [10] departed from the two models in determining the slip ratio k. He used his method of momentum exchange to obtain a relation between void fraction and steam quality as given by Eq. (2.31). Thus, while Fauske and Moody found that the exit slip ratios as given by Eqs. (2.13) and (2.23) are independent of the steam quality x, Levy found that the slip ratio increases with steam quality. Levy [10] also found that the predicted critical flow rate agrees better with experiments if the stagnation enthalpy is computed according to the homogeneous model, i.e.

$$h_o = h_f(1-x) + hgx + G^2v_H^2/2g_cJ , \tag{2.37}$$

where $v_H = xv_g + (1-x)v_f$.

A comparison of results based on the three critical flow models to those of James' empirical method are shown in Table 1. Note that although the James' formulae were obtained for lip pressure below 64 psia, it is shown that they are in good agreement with the results based on theoretical predictions even above 64 psia. In fact, results based on James' method are within 8% deviation with the results based on the three theoretical models for the whole range of lip pressure considered.

Table 1

COMPARISON OF RESULTS OBTAINED BASED ON JAMES' METHOD AND OTHER THEORETICAL MODELS

Case #	p (psia)	w $\left(\frac{\text{lbm}}{\text{ft}^2\cdot\text{sec}}\right)$	h_o $\left(\frac{\text{Btu}}{\text{lbm}}\right)$	G_M $\left(\frac{\text{lbm}}{\text{ft}^2\cdot\text{sec}}\right)$	x	Method
1	14.7	40	800.0	95.1	0.58	James (J)
			736.9	88.4	0.54	Fauske (F)
			749.0	89.9	0.55	Moody (M)
			745.4	91.8	0.54	Levy (L)
2	25.0	85.5	750.0	170.0	0.50	J
			698.7	164.5	0.48	F
			711.1	167.9	0.49	M
			724.2	171.2	0.50	L
3	60.0	226.0	715.0	415.4	0.46	J
			697.7	403.3	0.44	F
			709.9	412.0	0.45	M
			734.8	423.9	0.48	L
4	100.0	105.0	985.0	476.6	0.78	J
			1004.5	419.8	0.75	F
			1005.5	425.2	0.75	M
			1014.9	432.6	0.76	L
5	150.0	53.0	1130.0	590.0	0.90	J
			1148.8	523.4	0.90	F
			1149.7	528.9	0.90	M
			1151.8	538.6	0.90	L

It is important to note while Moody [8] and Levy [10] assumed isentropic flow in their models, this assumption was not being made in Fauske's model [6,7]. For this reason, Fauske's model can be used to determine the pressure gradient behavior in the approach region to the critical flow as will be discussed in Chapter V.

THE EFFECT OF NON-CONDENSIBLE GASES ON THE WELLBORE DISCHARGE CHARACTERISTICS

3.1 Background

In a hot water geothermal area, the presence of gases (such as CO_2) in the discharge from the wells or fumaroles has been found quite common, e.g., the Wairakei geothermal field in New Zealand and the Larderello geothermal field, in Italy. These non-condensible gases in the steam have an influence on the designed condenser pressure and therefore on the power output [13,14]. The presence of non-condensible gases affects the critical discharge pressure of steam due to the partial pressure of gases present in the gaseous phase of the two-phase flow. James [14] altered his empirical method [4] in order to take into account the change of steam pressure as follows: The measured lip pressure p is amended to a smaller value according to an empirical formula

$$p' = p(1-y/3.2) \ , \qquad (3.1)$$

where p' is the amended pressure psia, and

$$y = \frac{\text{weight of } CO_2 \text{ present in steam phase}}{\text{weight of steam}} . \qquad (3.2)$$

The usual procedure for the determination of G and h_0 are followed with the new value of p' and the measured weir flow rate.

In order to evaluate this modified method, Fauske's model [6] will now be extended to include effects of the extra components in gaseous phase of the two-phase flow. A comparison of the results with James' modified method will aso be made later in this chapter.

3.2 The Extension of Fauske's Model

In this section, we shall extend Fauske's one-component two-phase model to include the presence of the non-condensible gases. From the gas solubility charts given by Ellis [15], it can be concluded that the mass distribution of all the non-condensible gases present in the geothermal fluid lie mainly in the vapor phase. Moreover, as water starts flashing in the wellbore, most of the gases dissolved in the fluid are liberated into vapor phases. In the following we shall assume that the fraction of CO_2 gas present in the steam-water mixture is constant in the wellbore. As in the Fauske's original two-phase flow model, an annular flow pattern will be assumed where CO_2 gas and the steam will be moving with the velocity u_g while that of the liquid is uf (see Fig. 11). If σ is the fraction of the CO_2 gas present with respect to unit mass of steam and water, it follows that

$$\sigma \equiv \frac{\dot{m}_{CO_2}}{\dot{m}_g+\dot{m}_f} \ , \qquad (3.2a)$$

$$\sigma = xy \ , \qquad (3.2b)$$

where $x \equiv \frac{\dot{m}_g}{\dot{m}_g+\dot{m}_f}$, (3.2c)

with $\dot{m}_{CO_2}$, $\dot{m}_g$, and $\dot{m}_f$ denoting the mass flow rate of CO_2, vapor and liquid respectively. With the aid of the continuity equation

$$GA = \dot{m}_{CO_2} + \dot{m}_g + \dot{m}_f \ . \qquad (3.3)$$

It can be shown from Eqs. (3.2) that

$$\dot{m}_{CO_2} = \frac{\sigma GA}{(1+\sigma)} \ , \qquad (3.4a)$$

$$\dot{m}_g = \frac{xGA}{(1+\sigma)} \ , \qquad (3.4b)$$

$$\dot{m}_f = \frac{(1-x)GA}{(1+\sigma)} \ . \qquad (3.4c)$$

The momentum equation for the two-component, two-phase mixture is

$$\frac{dp}{dz} + \frac{1}{Ag_c}\frac{d}{dz}\left[(\dot{m}_{CO_2} + \dot{m}_g)u_g + \dot{m}_f u_f\right] + \frac{dF}{dz} = 0 \ . \qquad (3.5)$$

From Eqs. (3.4), it can be shown that

$$u_g = \frac{(x+\sigma)Gv_m}{\alpha(1+\sigma)} \ , \qquad (3.6a)$$

$$u_f = \frac{(1-x)Gv_f}{(1+\sigma)(1-\alpha)} \ , \qquad (3.6b)$$

where

$$v_m = v_g v_{CO_2}/(v_g + v_{CO_2}) \ . \qquad (3.7)$$

Eliminating G from Eqs. (3.6a) and (3.6b) and solving for α, we have

$$\alpha = \frac{(x+\sigma)v_m}{(1-x)v_f k + (x+\sigma)v_m} \ . \qquad (3.8)$$

Substituting Eqs. (3.4), (3.6) and (3.8) into Eq. (3.5) leads to

$$\frac{dp}{dz} = -\frac{G^2}{g_c}\left[\frac{dv}{dz} + \frac{fv}{2D}\right] \ , \qquad (3.9a)$$

where

$$v = \frac{(1-x)[(x+\sigma)v_m + k(1-x)v_f]}{(1+\sigma)^2 k} + \frac{(x+\sigma)[(x+\sigma)v_m + k(1-x)v_f]}{(1+\sigma)^2} \ . \qquad (3.9b)$$

It follows from Eqs. (3.9) that $\frac{dp}{dz}$ is a function of G, x, σ and k. Fauske proposed that $\frac{dp}{dz}$ is maximum for the critical flow occur. Thus, for fixed values of G, x, and σ, the critical condition is therefore

$$\frac{\partial}{\partial k}\left(\frac{dp}{dz}\right)_{G,x,\sigma} = 0 \ . \qquad (3.10)$$

Differentiating Eq. (3.9a) with respect to k according to Eq. (3.10) leads to Eqs. (2.11), (2.12a) and (2.12b). The condition of Eq. (2.12a) gives

$$k_M = \sqrt{\frac{v_m}{v_f}} \ . \qquad (3.11)$$

Integrating Eq. (3.9) and making use of the critical condition $\frac{dG}{dp} = 0$ yields

$$G_M = (1+\sigma)[-g_c/(a+b)]^{1/2} \ , \qquad (3.12)$$

where

$$a = \frac{dx}{dp}\{[-2(1-x) + k(1-2x-\sigma)]v_f + [(1-2x-\sigma)/k + 2(x+\sigma)]v_m\} \ ,$$

$$b = \frac{dv_m}{dp}\left[(1-x)(x+\sigma)/k + (x+\sigma)^2\right] \ .$$

Note that since $\frac{dv_f}{dp}$ is small in comparison with $\frac{dv_m}{dp}$, the term $\frac{dv_f}{dp}$ has been neglected in Eq. (3.12).

The stagnation enthalpy h_0 can be calculated based on the homogeneous flow model as follows.

$$h_0 = \left[h_f(1-x) + h_{CO_2}\sigma + h_g x + \frac{G^2 v_H^2}{2g_c J}\right] \ , \qquad (3.13)$$

where $v_H = \{v_f(1-x) + v_m(x+\sigma)\}/(1+\sigma)$. (3.14)

The weir flow rate w is expressed as,

$$w = G_M(1-x)/(1+\sigma) \ . \qquad (3.15)$$

For the special case of $\sigma = 0$, Eqs. (3.2)-(3.15) reduces to Fauske's model discussed in section 2.2.

The enthalpy of the liquid and steam phases can be calculated using the subprogram WASP [16], whereas the enthalpy of CO_2 can be calculated by integrating the specific heat correlation [18], i.e.,

$$\Delta h_{CO_2} = \int c_p(T)dT \ , \qquad (3.16)$$

$$\text{with} \quad c_p = 16.2 - \frac{6.53(10)^3}{T} + \frac{1.41(10)^6}{T^2} \ . \qquad (3.17)$$

where c_p is in BTU/mole-°F and T in degree Rankine.

The partial pressure (in lb_f/ft^2) of CO_2 according to the ideal gas law is,

$$P_{CO_2} = \frac{35.11\ Ty}{(144.0)v_g} \ , \qquad (3.18)$$

where v_g and T are respectively the specific volume (ft^3/lb_m) and saturation temperature corresponding to p_g. The partial pressures of CO_2 and

steam phase are added up to give the pressure p of the liquid phase, as

$$p = p_{CO_2} + p_g = \frac{35.11\ Ty}{144\ v_g} + p_g \ . \qquad (3.19)$$

For given values of p_g and y, the lip pressure p can be calculated according to Eq. (3.19). We now attempt to find a relationship between p_g and p in a form similar to Eq. (3.1). To this end, we shall assume the functional relationship between p_g and p as

$$p_g = p(1-y/m) \ , \qquad (3.20)$$

which can be solved for m to give

$$m = \frac{py}{p-p_g} \qquad (3.21)$$

For prescribed values of y and p_g, p can be found from Eq. (3.19) while m is determined from Eq. (3.21). The computed results for m versus p for selected values of y are presented in Fig. 12. It is noted from the figure that the value of m can be fitted by two straight lines as

$$m = [2.4 - 9.6(10^{-4})(p-14.7) + y] \ ,$$
$$\text{for } 14.7 \leq p \leq 100 \text{ psia} \qquad (3.22)$$

and

$$m = [2.378 - 7.7(10^{-4})(p-100.0) + y] \ ,$$
$$\text{for } 100 \leq p \leq 200 \text{ psia.} \qquad (3.23)$$

For the lip pressures in the range of 14.7 psia to 150 psia and at different values of y, p_g can be computed according to Eq. (3.20) while G_M, h_o, and w can be computed according to Eqs. (3.12), (3.13) and (3.15). The results of the computations are presented in Figs. 13-18, where the steam pressure p_g is used as one of the variables in the plots.

3.3 Results and Discussion

For a given set of values of lip pressure and weir flow rate, Table II shows that the effects of the presence of CO_2 gas are:

1. The total mass flow rate G decreases.
2. The vapor pressure is smaller in magnitude than that of the lip pressure because of the partial pressure of CO_2 gas.
3. The specific enthalpy of the vapor phase is smaller due to the reduced vapor pressure as well as the reduction of steam content as a result of the presence of the non-condensible gas.

A comparison of results Based on the modified James' method to the theoretical predictions based on the present work is presented in Table III. It is shown that the modified James' method gives a higher critical flow rate than that of the theoretical predictions based on the extension of Fauske's model. Since it was found in Chapter II that the critical flow rates given by the three models do agree within 8% with each other, no effort will be made for the extension of other models for the investigation of the effects of non-condensible gases.

THE EFFECT OF DISSOLVED SOLIDS ON THE WELLBORE DISCHARGE CHARACTERISTICS

4.1 Background

In a hot water geothermal area, the presence of dissolved solids in the discharge of the wells has also been found of common occurrence, e.g. as much as 30% in the Salten Sea geothermal fields. Since all three two-phase critical models give the critical mass flow rates within 8% with each other, only Fauske's model [6] will be used to investigate the effects of dissolved solids on wellbore flow characteristics in this chapter. As sodium chloride proportion is quite large in the portion of dissolved solids, it introduces little error to assume that sodium chloride is the only solid dissolved in the wellbore discharge water.

4.2 An Extension of Fauske's Model

Fauske's model as described in section 2.2 will now be extended to include dissolved salts. The governing equations are the same as those in section 2.2 except that instead of a steam table, properties of saturated brine will be used for computation. The saturation properties of brine solution are calculated using the simple method given by Dittman [19] with the aid of a WASP subprogram [16]. It is assumed that the dissolved salt does not precipitate in the wellbore. The mass flow rate G, weir flow rate w (which contains dissolved salt), and stagnation enthalpy h_o of the brine solution were computed for a range of lip pressures from 14.7 psia to 150 psia. The results are plotted in Figs. 19-28 for various weight percentages of the salt in the brine solution.

4.3 Results and Discussion

For a set of readings of lip pressure (p) and, weir flow rate (w), and salt content (by weight percentage) in the discharge (as determined from a chemical analysis), the corresponding mass flow rate, the stagnation enthalpy, and steam quality can be determined from Figs. 19-28. Note that the precipitation of the salt in the steam separator may result in weir flow of less salt content. Thus, the weir flow rate readings must be corrected before using Figs. 19-28, which are computed for the particular salt content at the critical flow cross section.

The effects of dissolved salt on the flow rate, steam quality, and weir flow rate for the same lip pressure and stagnation temperature are reported in Table IV. It is shown that with the increase of salt content, both the total flow rate and the weir flow rate increase while the exit steam quality decreases. For a geothermal field such as the Imperial Valley where 30% dissolved salt exists in the wellbore, its effect on the total mass flow rate and exit steam quality is quite significant, as is shown in Table IV.

Table II

EFFECTS OF CO_2 ON THE WELLBORE DISCHARGE CHARACTERISTICS

p_f (psia)	w $\left(\frac{lbm}{ft^2 \cdot sec}\right)$	y	G_M $\left(\frac{lbm}{ft^2 \cdot sec}\right)$	p_g (psia)	h_g $\left(\frac{Btu}{lbm}\right)$	x
15.0	107.5	0.0	153.9	15.0	1150.9	0.30
		0.05	153.6	14.7	1150.5	0.29
26.0	30.0	0.0	116.6	26.0	1161.5	0.74
		0.1	112.4	25.0	1160.7	0.71
16.0	40.0	0.0	92.6	16.0	1152.1	0.57
		0.2	89.5	14.7	1150.5	0.51
54.0	100.0	0.0	270.2	54.0	1175.6	0.63
		0.2	258.3	50.0	1174.1	0.57
156.0	670	0.0	1090.0	156.0	1194.7	0.38
		0.1	1084.3	150.0	1194.1	0.36

Table III

COMPARISON OF RESULTS BASED ON THE MODIFIED JAMES' METHOD AND THE MODIFIED FAUSKE'S MODEL FOR WELLBORE DISCHARGE WITH CO_2

w $\left(\frac{lbm}{ft^2 \cdot sec}\right)$	p (psia)	y	G_M $\left(\frac{lbm}{ft^2 \cdot sec}\right)$	Method
50.16	15.01	0.05	89.42	Modified James' Method (MJ)
			79.68	Modified Fauske's Model (MF)
255.66	54.21	0.2	446.0	MJ
			413.71	MF

Table IV

EFFECTS OF DISSOLVED SALTS ON THE WELLBORE DISCHARGE CHARACTERISTICS

p (psia)	T_0 (F°)	Salt % by Weight	G_M $\left(\frac{lbm}{ft^2 \cdot sec}\right)$	w $\left(\frac{lbm}{ft^2 \cdot sec}\right)$	x
60.00	500	0	659	507	0.23
		5	663	570	0.23
		10	737	589	0.20
		15	799	655	0.18
		20	860	720	0.16
		25	915	778	0.15

THE EFFECTS OF LIP PRESSURE TAPPING POSITION AND PIPE DIAMETER

5.1 Background

The accurate lip pressure measurements are of crucial importance for the determination of wellbore discharge characteristics in James' method. Since it is impossible to measure lip pressure precisely at the critical flow at the exit, James suggested to take the lip pressure measurements exactly 1/4" away from the exit in order to make the method consistent for use. In order to investigate the effects of the pressure tapping position and the diameter of the horizontal pipe on the lip pressure measurements, it is important to know the pressure drop behavior especially in the approach region to the critical flow.

It should be noted that the pressure drop behavior is due to friction and momentum losses. Thus, Moody's and Levy's models cannot be used for analysis because they assumed the isentropic flow behavior. This assumption was not made in Fauske's model, thus allowing the prediction of the pressure drop behavior in the approach region to critical flow.

The procedures employed by Fauske for the investigation of pressure gradients in a pipe is as follows. First, the critical mass flow rate is computed according to Section 2.2. Equations (2.7a) and (2.8) are then integrated numerically with the void fraction and steam quality given by Eq. (2.14). The friction factor for Eq. (2.7a) was obtained by Fauske based on his own experimental data for the approach region to the two-phase critical flow. Fauske's approach has been subjected to criticism for the following reasons [20]: (1) Fauske's friction factor correlation is a function of quality only and hence is probably restricted to pipe geometries and conditions employed in the test apparatus, (2) the void fraction and steam quality relation given by Eq. (2.14) is only valid in the region close to the critical flow cross section, and (3) no correlation for friction factor is provided for further upstream region.

An improved method has been suggested by Nahavandi and Von Hollen [20] who employed the modified Armand void fraction

$$\alpha = \left[\frac{0.833 + 0.167x}{xv_g + (1-x)v_f}\right] xv_g \ , \qquad (5.1)$$

when performing the numerical integration of Eq. (2.7a). The method uses an iterative procedure for the numerical integration of the governing equations to determine the critical mass flow rate while finding the pressure and local steam quality in the process. As an input to the method, the knowledge of upstream conditions is required in order to calculate the pressure drop behavior and the critical mass flow rate.

In the present work we would like to study the pressure gradient behavior for exit pressures in the range of 14.7 psia to 150 psia with pipe diameters of 3", 6" and 8" (which were the pipe diameters used in James' experiments). To perform the analysis, Nahavandi and Von Hollen's method will be combined with Fauske's, thus allowing the accurate calculations of pressure gradients in terms of exit pressures.

5.2 Analysis of Pressure Drop Behavior

The governing equations adopted will be the same as Fauske's i.e., Eqs. (2.7)-(2.18). However, when Eq. (2.7a) is integrated numericaly, the void fraction is not given by Eq. (2.14) but by Eq. (5.1) while the friction factor is determined from the standard plot [21] where the friction factor is a function of pipe roughness and the two-phase Reynolds number defined as

$$N_R = GD[x/\mu_g + (1-x)/\mu_f] \ , \qquad (5.2)$$

where μ_g and μ_f are the dynamic viscosity of vapor and liquid respectively. For given values of lip pressure and steam quality at the exit (i.e., at z'=0), the numerical integration of Eq. (2.7a) will be proceeded as follows: (i) calculate the mass flow rate using Fauske's model as described in Section 2.2; (ii) calculate h_o from Eq. (2.6b), and (iii) for a given pressure greater than the lip pressure, the corresponding distance Δz from the critical flow cross section upstream can be computed by integrating Eq. (2.7a) with void fraction given by Eq. (5.1), if the local steam quality upstream is known. To determine the upstream steam quality, an iterative process will be used to solve the following equation:

$$x = \frac{-b \pm \sqrt{b^2-4ac}}{2a} \ , \qquad (5.3)$$

with $a = G_M^2(v_g-v_f)^2/2g_cJ$,

$b = h_{fg} + G_M^2(v_f)(v_g-v_f)^2/2g_cJ$,

$c = -h_o + h_f + G_M^2/2g_cJ(v_f^2)$,

where the right-hand side of Eq. (5.3) can be evaluated if a trial value for the steam quality is assumed. An imporved value for x is then given by Eq. (5.3), which is the energy equation based on the homogeneous model. The simple homogeneous model for the computations of the stagnation enthalpy is adopted here because it is known that it compares better with experiments [10]. Note that choosing small pressure steps would lead to a better answer as the frictional drop term was approximated by the mean value for N_R and the v for the particular step. For geothermal applications, it is estimated that the friction factor is approximately equal to 0.015 from the chart given by Moody [21]. Computations for pressure distribution were obtained for exit pressures from 14.7 psia to 150 psia and with pipe diameters of 3" and 6". Results are presented in Tables V and VI. Pressure distribution for cases 1 and 4 in Table V and VI are plotted in Figs. 29 and 30 for comparison.

Table V

PRESSURE DISTRIBUTION IN THE APPROACH REGION TO CRITICAL FLOW IN A 3" PIPE

Case	x	p (psia)	z' (ft)
i	0.2	14.7	0
		16.1	0.98
		16.9	1.58
		17.6	2.49
ii	0.8	28.0	0
		27.5	1.17
		30.0	2.27
		31.2	2.98
iii	0.4	40.0	0
		44.0	1.11
		46.0	1.71
		48.0	2.37
iv	0.4	100.0	0
		105.0	0.31
		110.0	0.73
		115.0	1.36
		120.0	2.06

Table VI

PRESSURE GRADIENT BEHAVIOR IN THE APPROACH REGION TO CRITICAL FLOW IN A 6" PIPE

Case	x	p (psia)	z' (ft)
i	0.2	14.7	0
		16.1	1.97
		16.9	3.16
		17.6	4.98
ii	0.8	25.0	0.0
		27.5	2.35
		30.0	4.54
		31.2	5.96
iii	0.4	40.0	0.0
		44.0	2.22
		46.0	3.42
		48.0	4.74
iv	0.4	100.0	0.0
		105.0	0.624
		110.0	1.46
		115.0	2.73
		120.0	4.12

5.3 Results and Discussion

Figures 29 and 30 show that for the same lip pressure and exit steam quality, the pressure gradient at the exit is steeper for smaller diameter pipes. It can be concluded from these figures that if the pipe diameter is larger than 6", the lip pressure measured at 1/4" from the exit would not be significantly higher than that at the exit, thus will not affect the determination of the critical flow rate. However, significant errors in lip pressure measurements will be introduced if the pipe diameter is smaller than 6"; the errors increase as the lip pressure is increased.

CONCLUDING REMARKS

A theoretical study based on two-phase critical flow models has been performed to evaluate James' empirical method for the determination of geothermal wellbore discharge characteristics. The following conclusions are obtained:

1. The James' empirical method for the determination of stagnation enthalpy, steam quality, and total flow rate are within 8% from results predicted from one-component two-phase critical flow models of Fauske, Moody, and Levy.
2. When the wellbore discharge contains a substantial amount of CO_2, the determination of discharge characteristics based on the modified James' method agree with those predicted based on a modification of Fauske's model to the same degree of accuracy.
3. An extension of Fauske's theory shows that if a large amount of dissolved salts exist in the discharge, the straightforward application of James' method for the determination of discharge characteristics will lead to serious errors.
4. When the lip pressure is low and the discharge pipe diameter is equal to or larger than 6-inches in diameter, the pressure gradient in the approach region of the critical flow is small such that the lip pressure measurements taken within 1/4-inch from the exit would not affect the accuracy of the determination of the critical flow rate.

REFERENCES

1. Cheng, P., "Heat Transfer in Geothermal Systems," Advances in Heat Transfer, v. 14, p. 1 (1978).
2. James, R., "Possible Serious Effect of the Presence of Steam on Hot-Water Flow Measurements Utilizing an Orifice Meter," Proc. 2nd United Nations Symposium on the Development and Use of Geothermal Resources, v. 3, p. 1703, Lawrence Berkeley Laboratory, University of California (1975).
3. James R., "Steam-Water Critical Flow Through Pipes," Proc. Inst. Mech. Engrs., v. 176, p. 741 (1962).
4. James, R., "Measurement of Steam-Water Mixtures Discharging at the Speed of Sound to the Atmosphere," New Zealand Engineering, v. 2, Part 2, p. 1676 (1970).
5. Yuen, P.C. and et al., Hawaii Geothermal Project: Phase III - Well Testing and Analysis Report, July 1, 1977.
6. Fauske, H., "Contribution to the Theory of Two-Phase, One-Component Critical Flow," Argonne National Laboratory Report, #ANL-6633 (1962).
7. Fauske, H., "A Theory for Predicting Pressure Gradients for Two-Phase Critical Flow," Nucl. Sci. and Engg., v. 17, p. 1 (1963).

8. Moody, F., "Maximum Flow Rate of a Single Component Two-Phase Mixture," J. Heat Transfer, Trans. ASME, Series C., p. 134 (1965).

9. Levy, S., "Steam-Slip Theoretical Prediction from Momentum Model," J. Heat Transfer, Trans. ASME, Series C, v. 82, p. 113 (1960).

10. Levy, S., "Prediction of Two-Phase Critical Flow Rate," ASME Paper 64-HT-8.

11. Moody, F.J., "Maximum Discharge Rate of Liquid-Vapor Mixtures from Vessels," NEDO-21052, 75NED53, General Electric Co., (1975).

12. Keenan, J.H., Keyes, F.G., and Moore, J.G., Steam Tables, John Wiley & Sons, New York (1969).

13. James, R., "Power Station Strategy," Geothermics, Special Issue 2, v. 2, Part 2, p. 1676 (1970).

14. James, R., "Factors Controlling the Borehole Performance," Geothermics, Special Issue 2, v. 2, Part 2, p. 1502 (1970).

15. Ellis, A.J., "Interpretation of Gas Analysis from the Wairakei Hydrothermal Area," New Zealand Journal of Science, v. 5, p. 434 (1962).

16. Hendricks, R.C., Peller, I.C. and Baron, A.K., "WASP -- A Flexible FORTRAN IV Computer Code for Calculating Water and Steam Properties," NASA Lewis Research Center, NASA TN D-7391 (1970).

17. National Bureau of Standards Circular #564, Tables of Thermal Properties of Gases (1955).

18. Jones, J.B. and Hawkins, G.A., "Engineering Thermodynamics," John Wiley and Sons, New York (1960).

19. Dittman, G.L., "Calculation of Brine Properties," Lawrence Livermore Laboratory, UCID-17406 (1977).

20. Nahavandi, A., and Von Hollen, R.F., "Two Phase Pressure Gradients in the Approach Region to Critical Flow," Nucl. Sci. & Engg., v. 22, p. 463 (1965).

21. Moody, L.F., "Friction Factors for Pipe Flow," Trans. of ASME, p. 671 (1944).

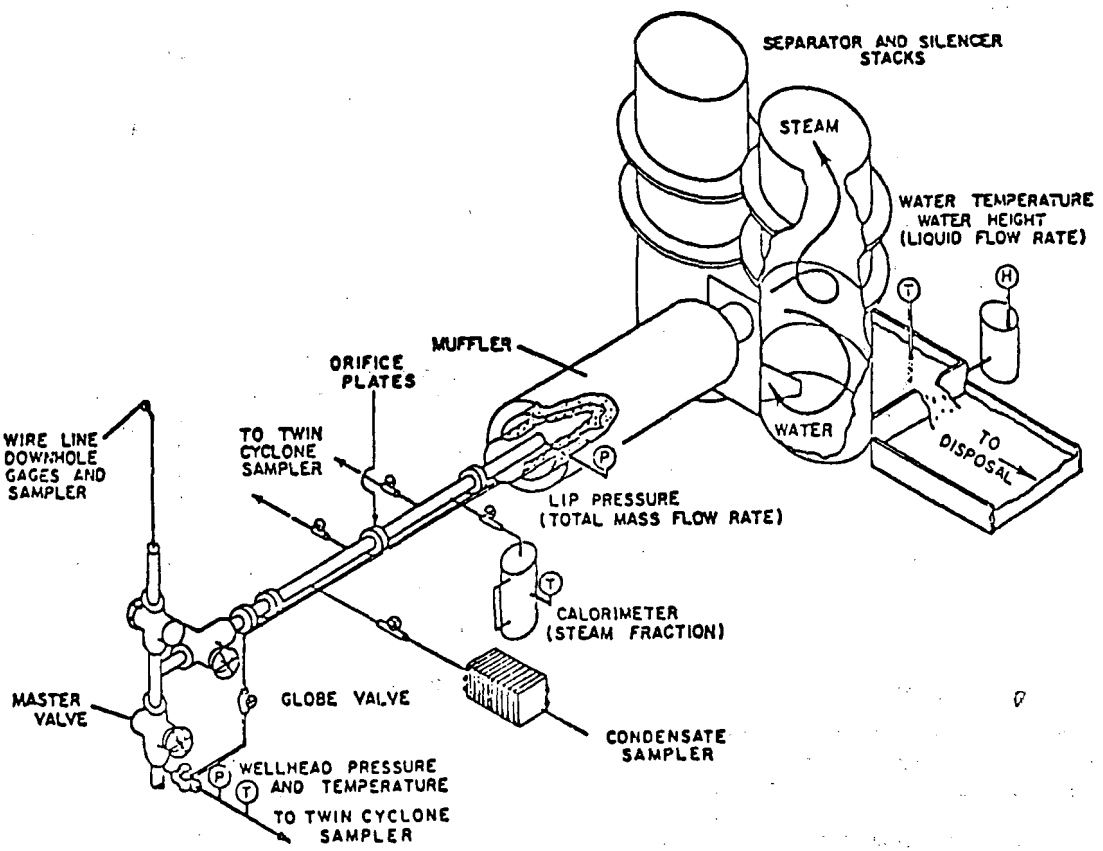

Fig. 1 A Typical Set-Up Required for James' Method on a Well Site [5]

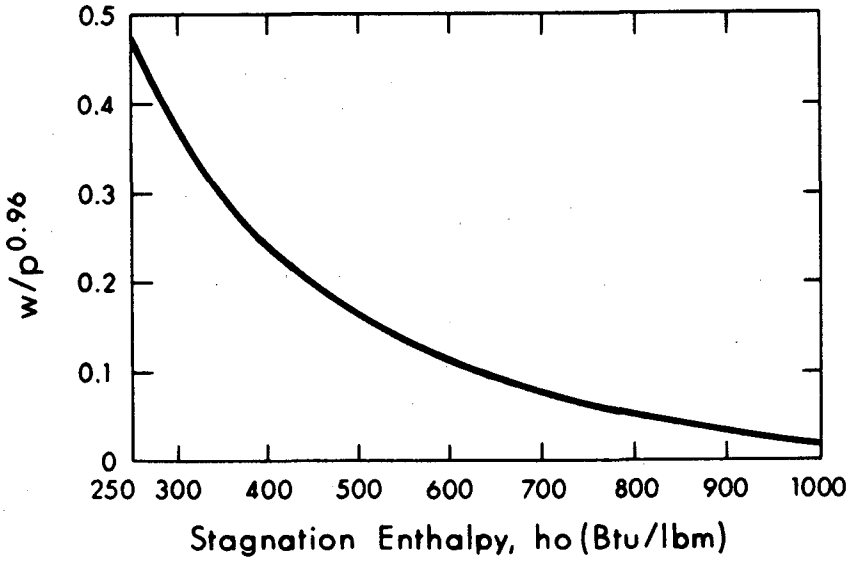

Fig. 2 Value of $w/p^{0.96}$ vs. h_0

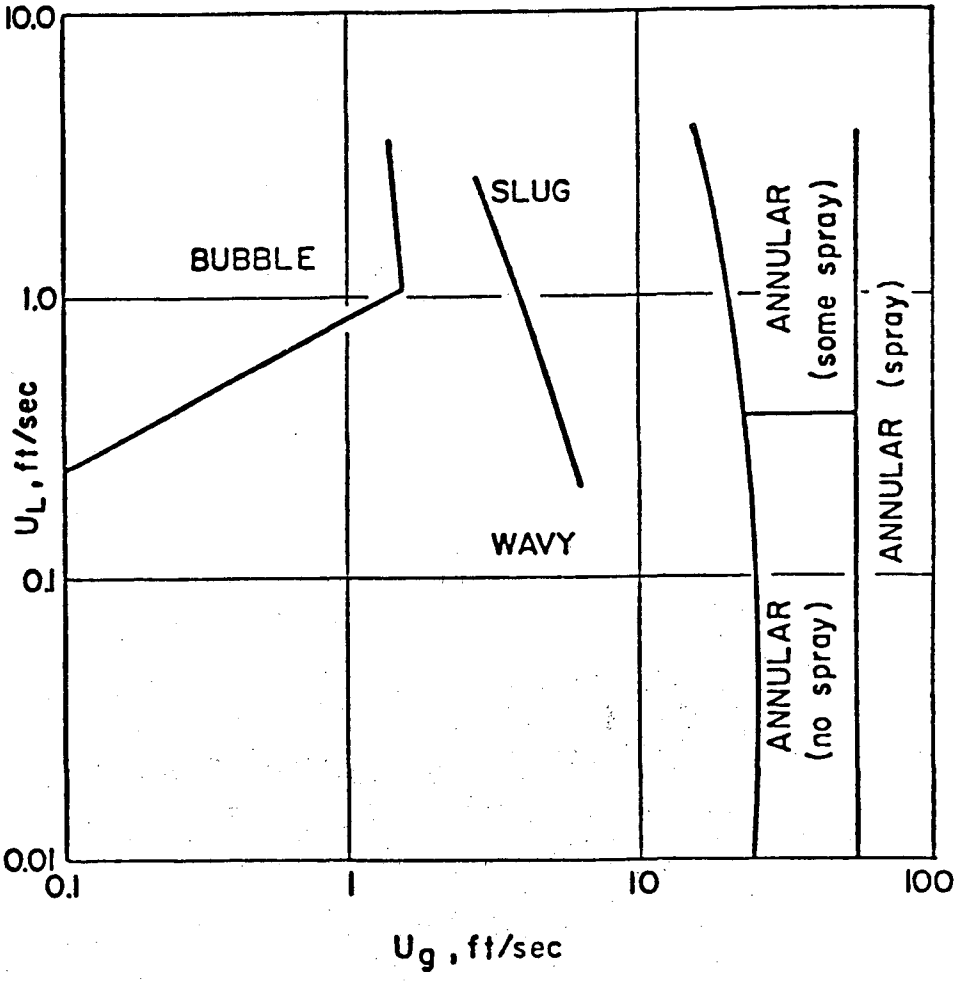

Fig. 3 Two-Phase Flow Regimes [6]

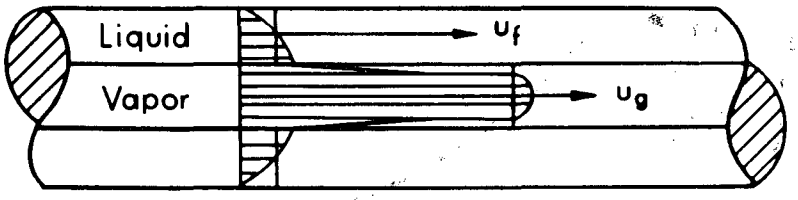

Fig. 4 Physical Pictures of Annular Two-Phase Flow [6]

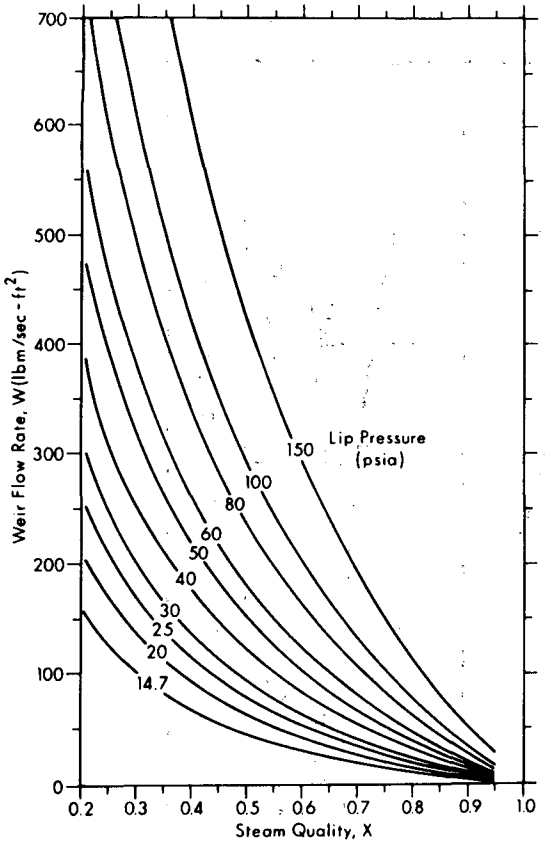

Fig. 5 Weir Flow Rate vs. Steam Quality at Selected Values of Lip Pressure According to Fauske's Model

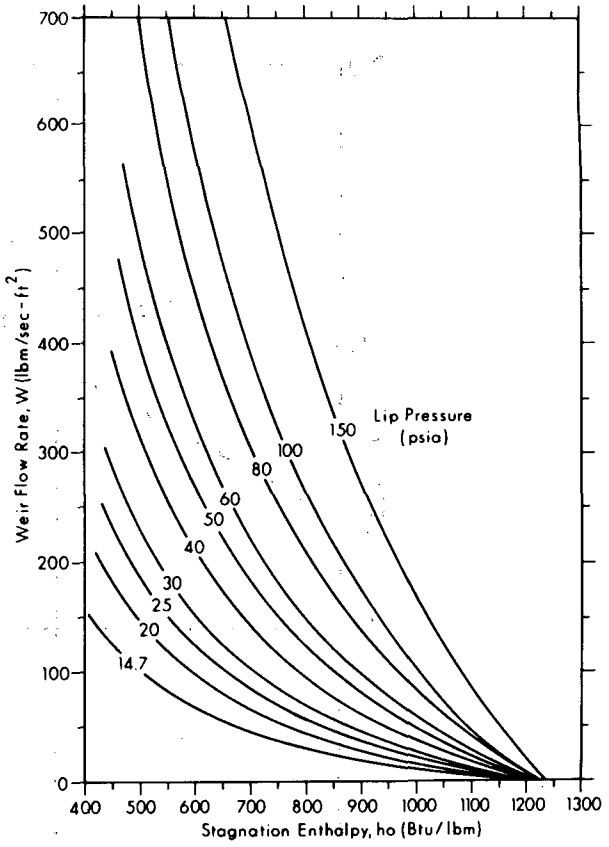

Fig. 6 Weir Flow Rate vs. Stagnation Enthalpy at Selected Values of Lip Pressure According to Fauske's Model

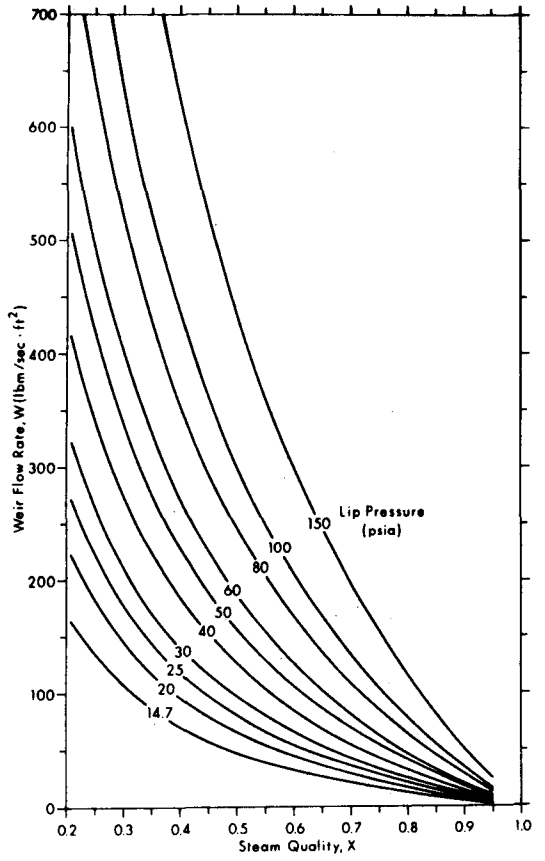

Fig. 7 Weir Flow Rate vs. Steam Quality at Selected Values of Lip Pressure According to Moody's Model

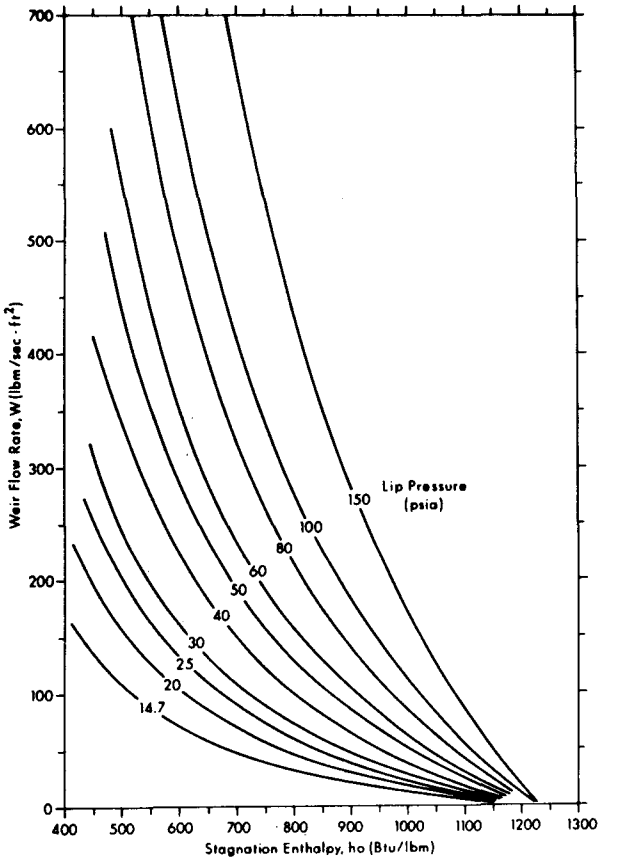

Fig. 8 Weir Flow Rate vs. Stagnation Enthalpy at Selected Values of Lip Pressure According to Moody's Model

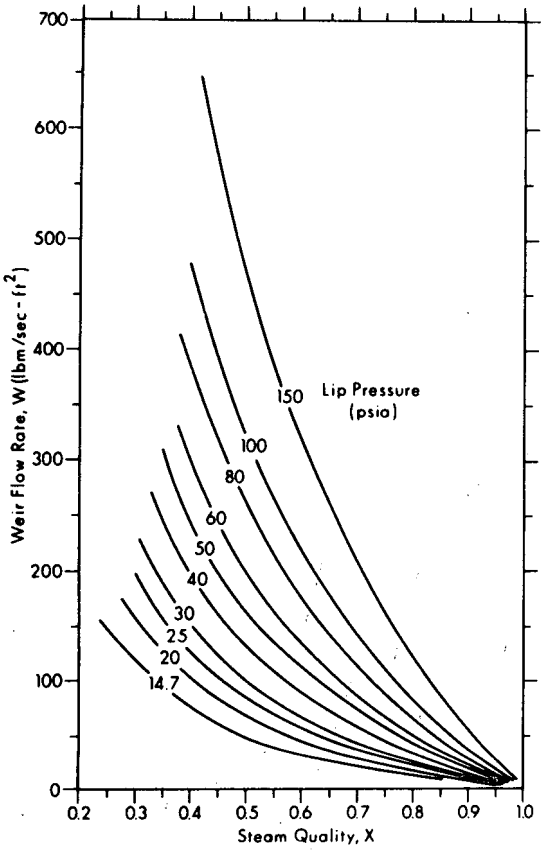

Fig. 9 Weir Flow Rate vs. Steam Quality at Selected Values of Lip Pressure According to Levy's Model

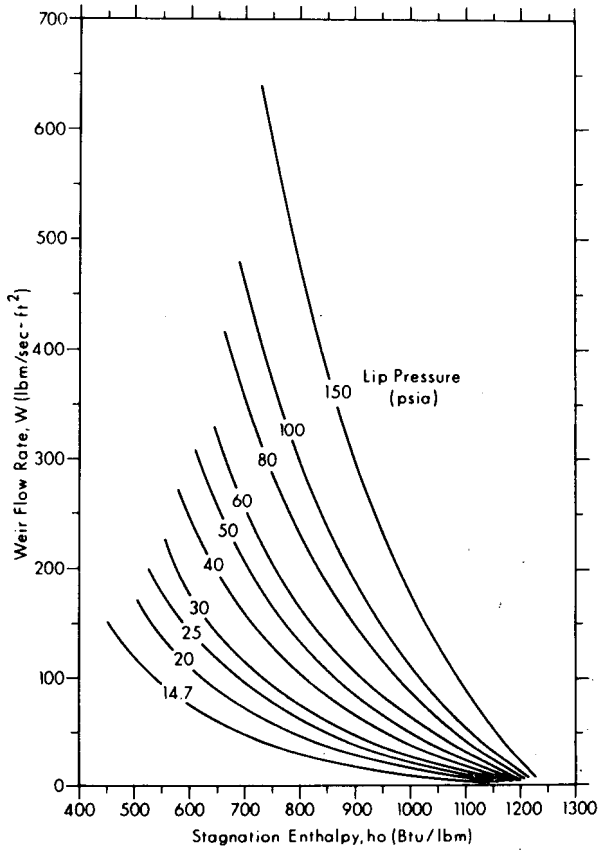

Fig. 10 Weir Flow Rate vs. Stagnation Enthalpy at Selected Values of Lip Pressure According to Levy's Model

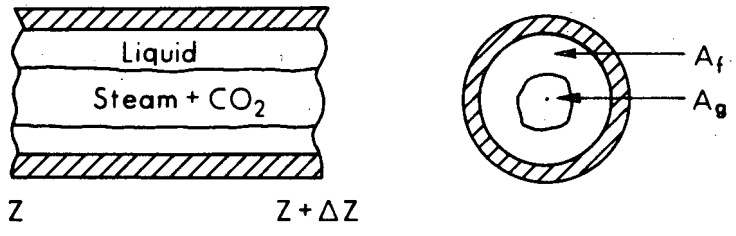

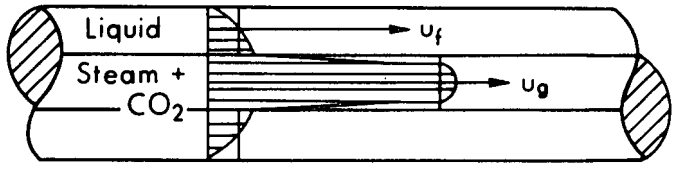

Fig. 11 Physical Pictures of Two-Component Two-Phase Annular Flow

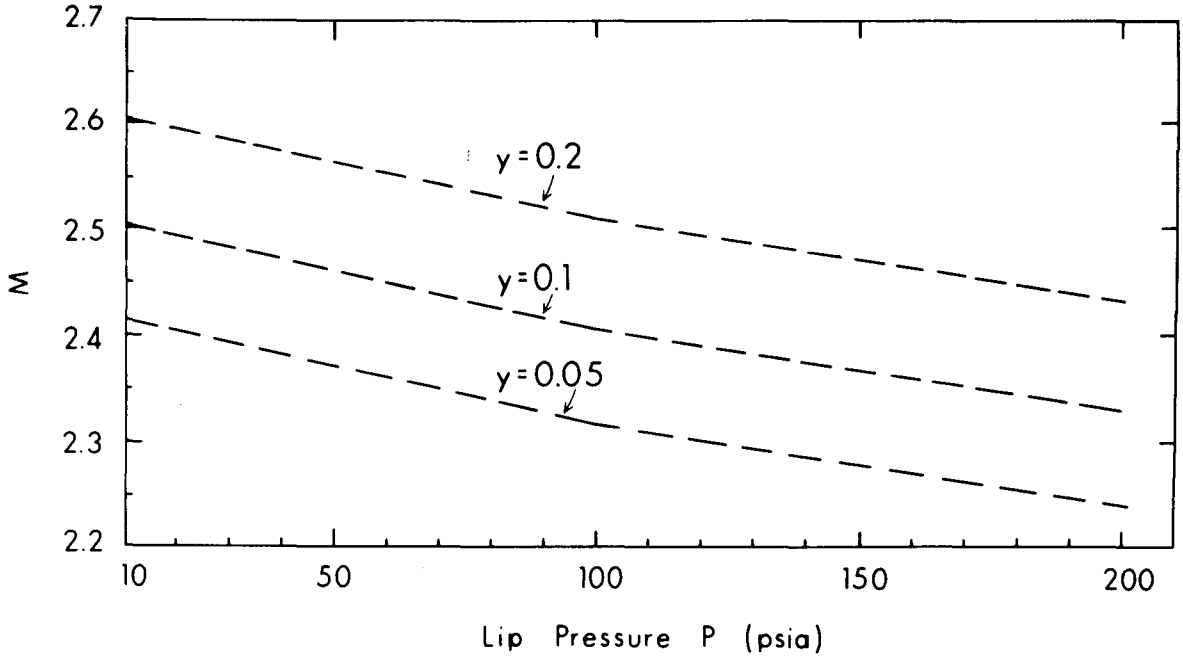

Fig. 12 Value of M vs. Lip Pressure at Selected Values of y

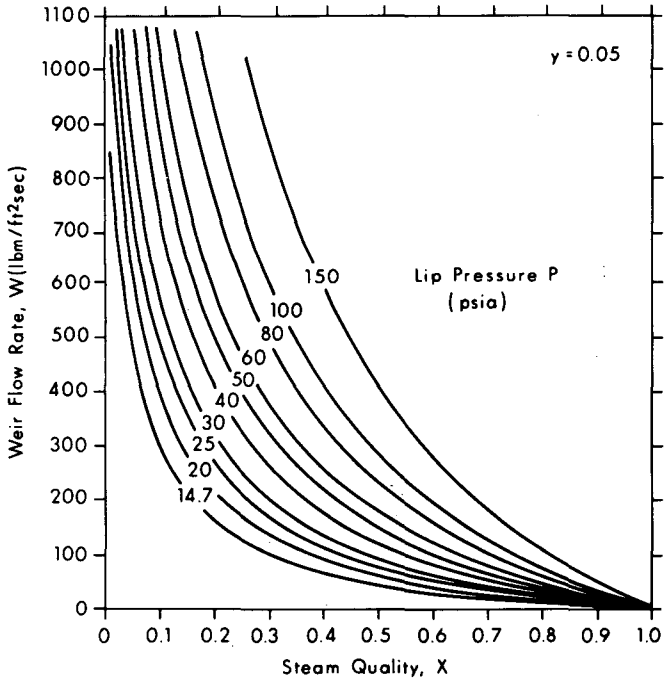

Fig. 13 Weir Flow Rate vs. Steam Quality for y = 0.05 at Selected Values of Steam Pressure

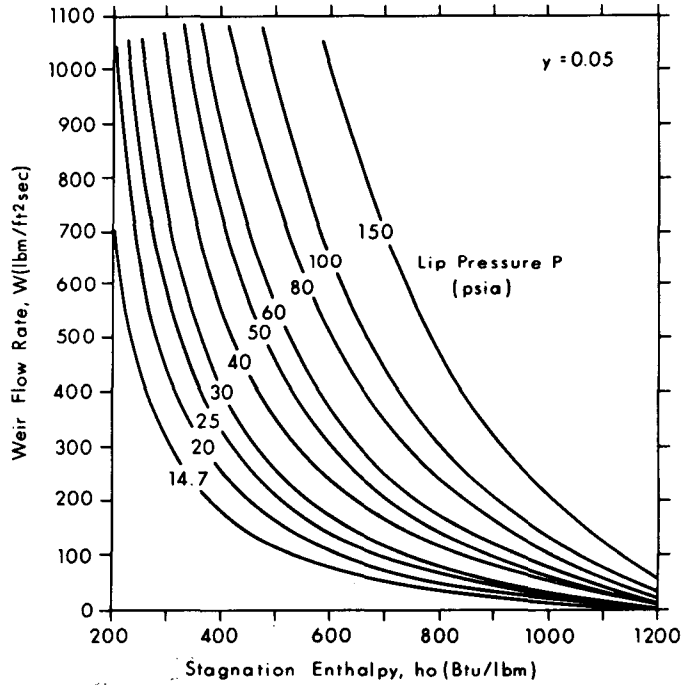

Fig. 14 Weir Flow Rate vs. Stagnation Enthalpy for y = 0.05 at Selected Values of Steam Pressure

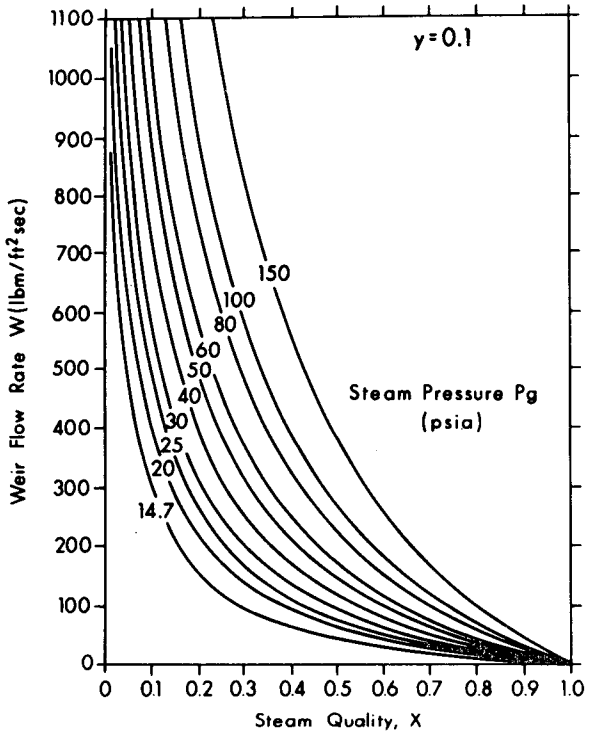

Fig. 15 Weir Flow Rate vs. Steam Quality for y = 0.1 at Selected Values of Steam Pressure

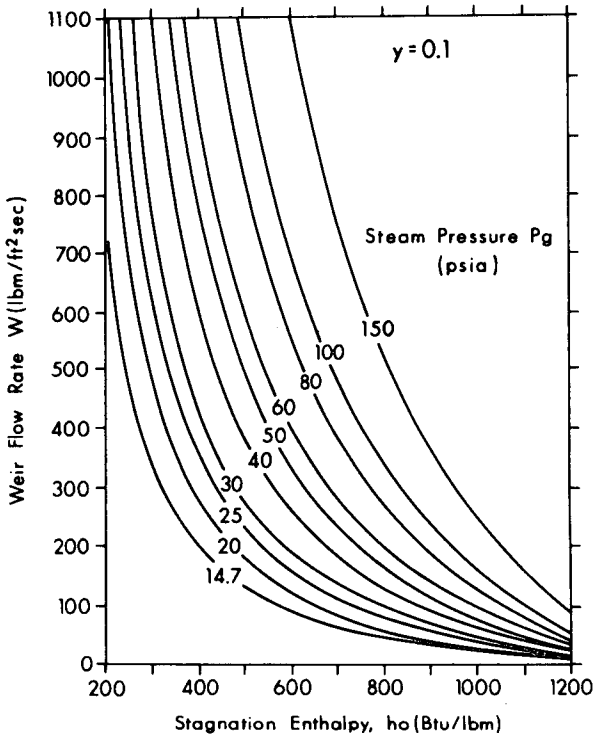

Fig. 16 Weir Flow Rate vs. Stagnation Enthalpy for y = 0.1 at Selected Values of Steam Pressure

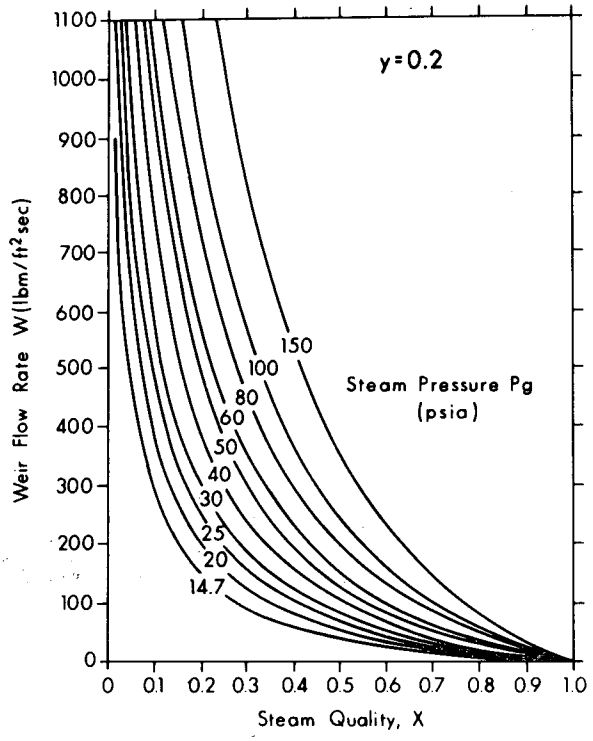

Fig. 17 Weir Flow Rate vs. Steam Quality for y = 0.2 at Selected Values of Steam Pressure

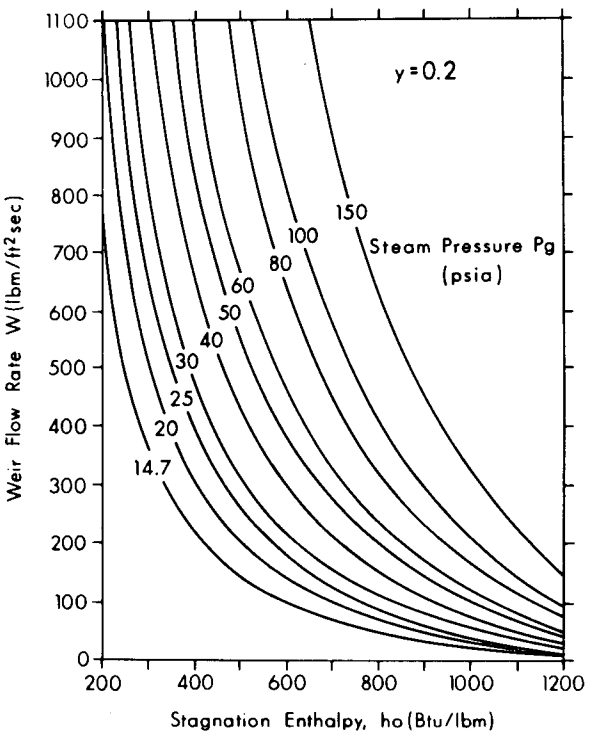

Fig. 18 Weir Flow Rate vs. Stagnation Enthalpy for y = 0.2 at Selected Values of Steam Pressure

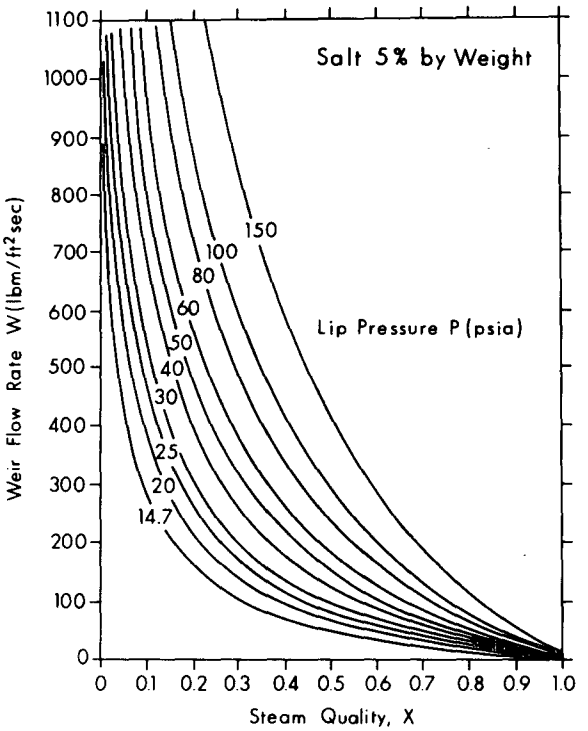

Fig. 19 Weir Flow Rate vs. Steam Quality for Brine with Salt Content of 5% by Weight

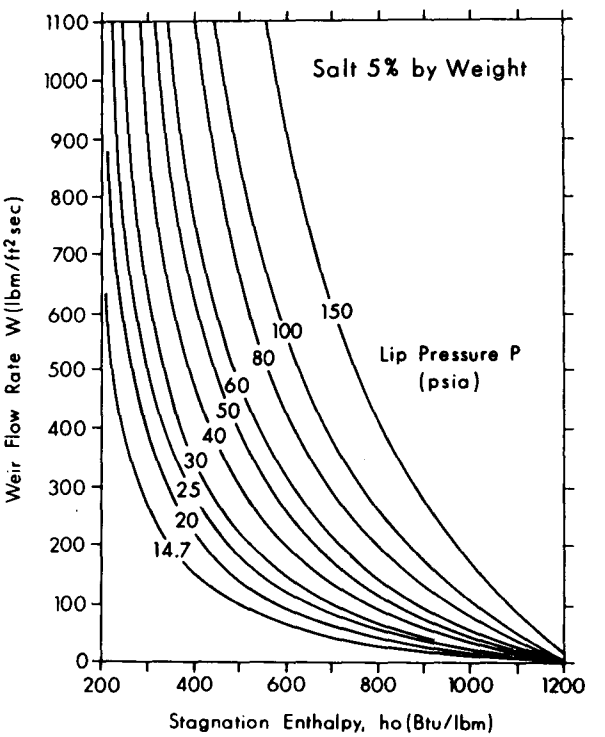

Fig. 20 Weir Flow Rate vs. Stagnation Enthalpy for Brine with Salt Content of 5% by Weight

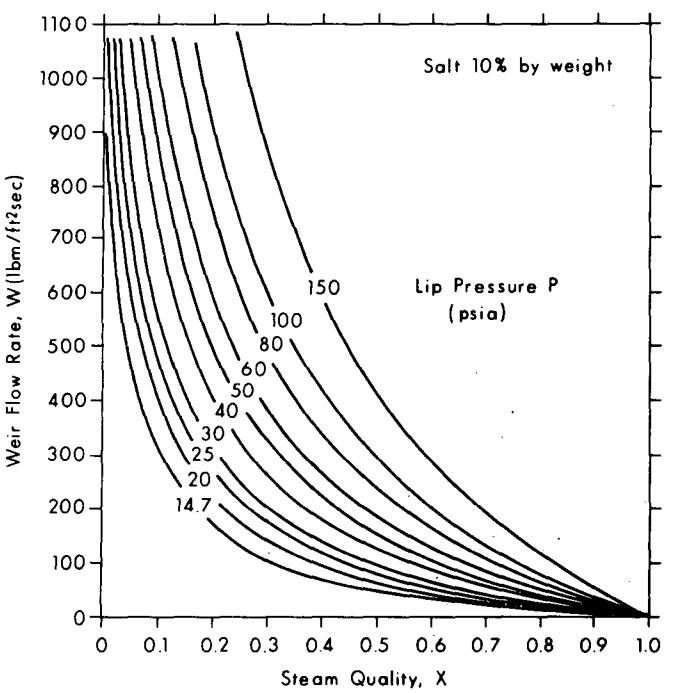

Fig. 21 Weir Flow Rate vs. Steam Quality for Brine with Salt Content of 10% by Weight

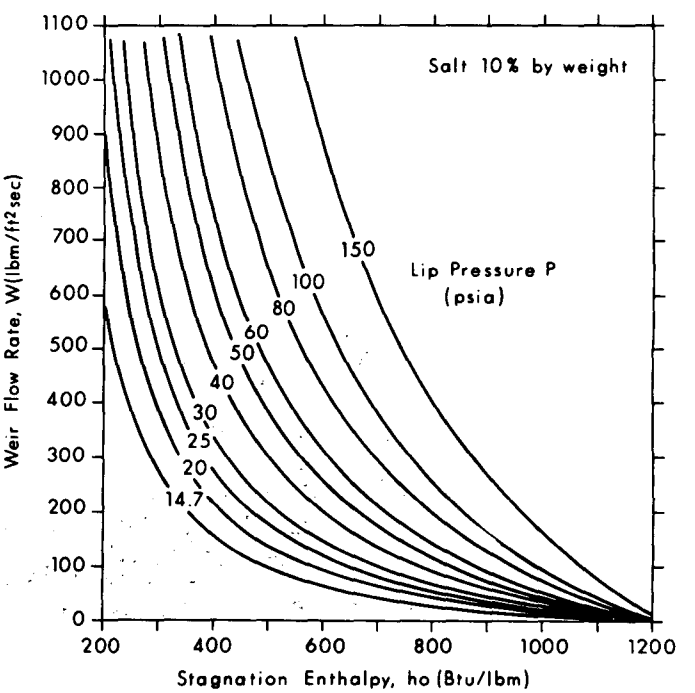

Fig. 22 Weir Flow Rate vs. Stagnation Enthalpy for Brine with Salt Content of 10% by Weight

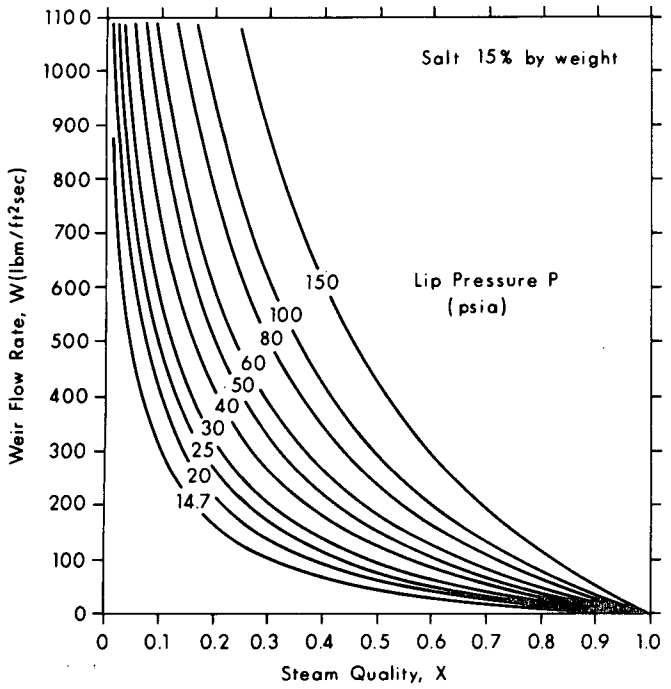

Fig. 23 Weir Flow Rate vs. Steam Quality for Brine with Salt Content of 15% by Weight

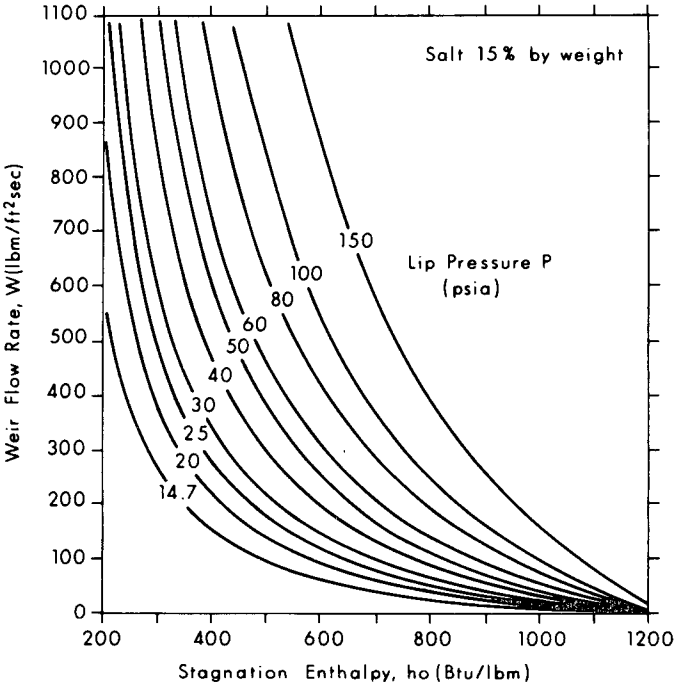

Fig. 24 Weir Flow Rate vs. Stagnation Enthalpy for Brine with Salt Content of 15% by Weight

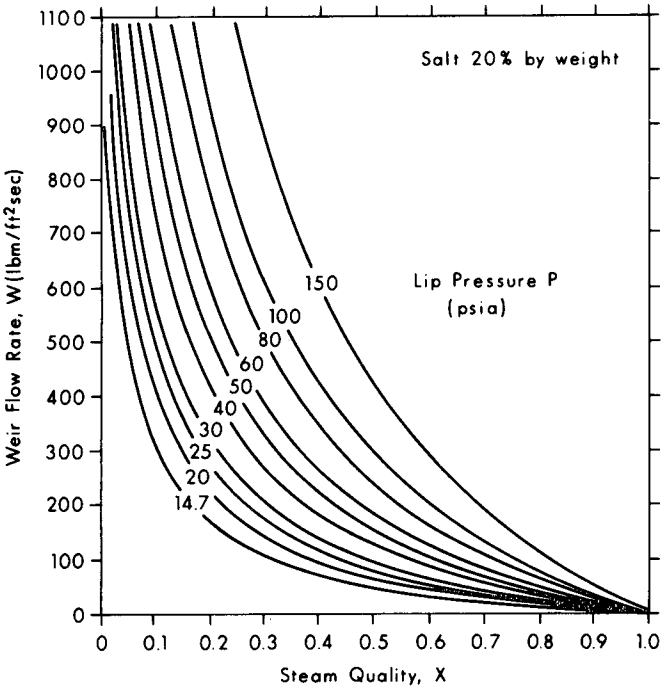

Fig. 25 Weir Flow Rate vs. Steam Quality for Brine with Salt Content of 20% by Weight

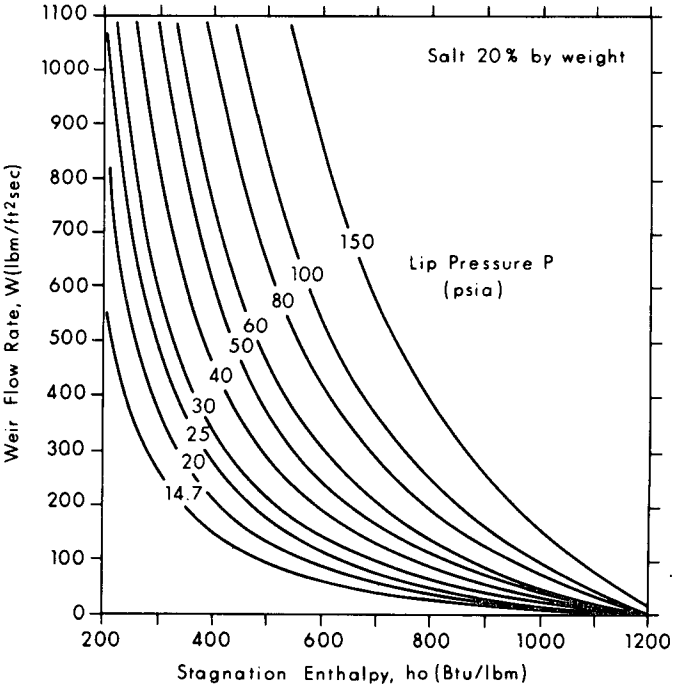

Fig. 26 Weir Flow Rate vs. Stagnation Enthalpy for Brine with Salt Content of 20% by Weight

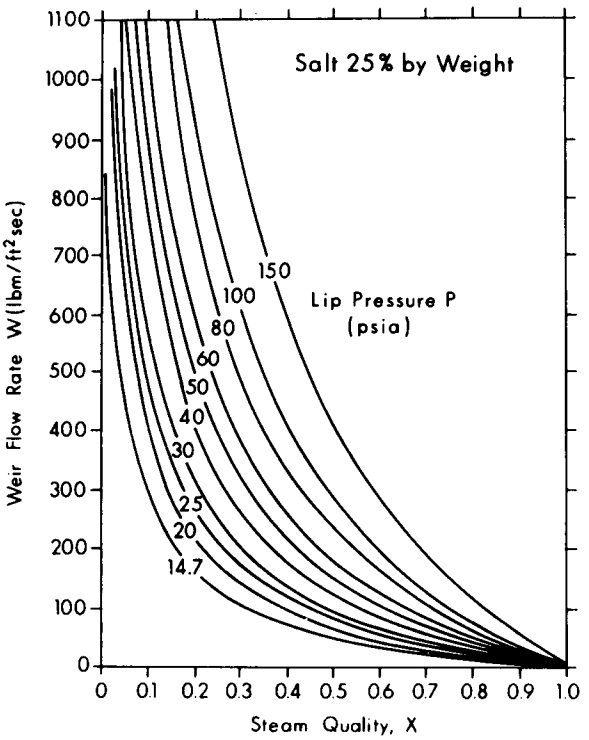

Fig. 27 Weir Flow Rate vs. Steam Quality for Brine with Salt Content of 25% by Weight

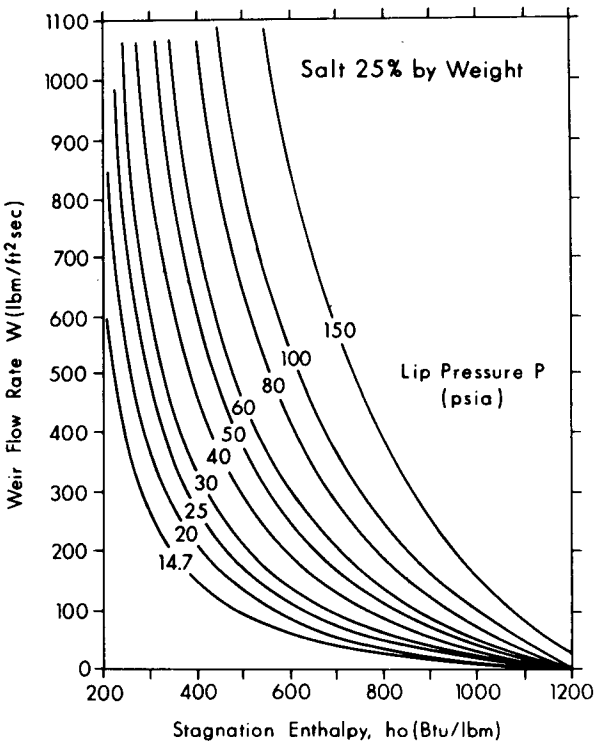

Fig. 28 Weir Flow Rate vs. Stagnation Enthalpy for Brine with Salt Content of 25% by Weight

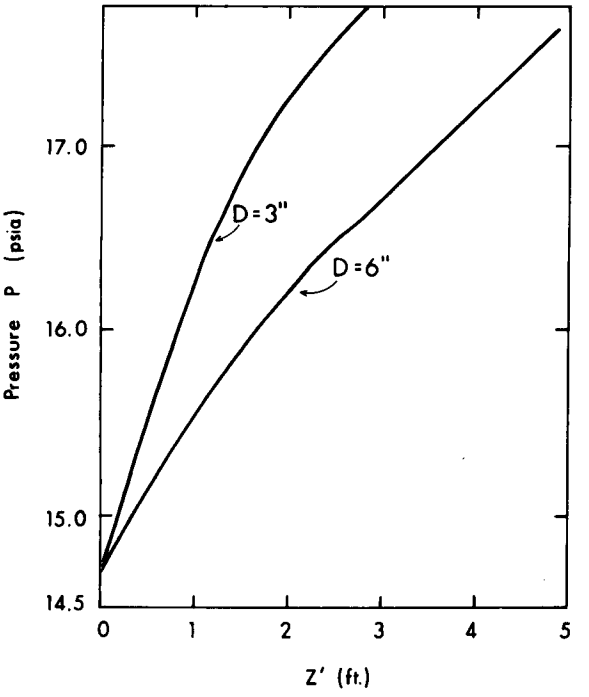

Fig. 29 Pressure Distribution in the Approach Region to Critical Flow with Lip Pressure at 14.7 psia

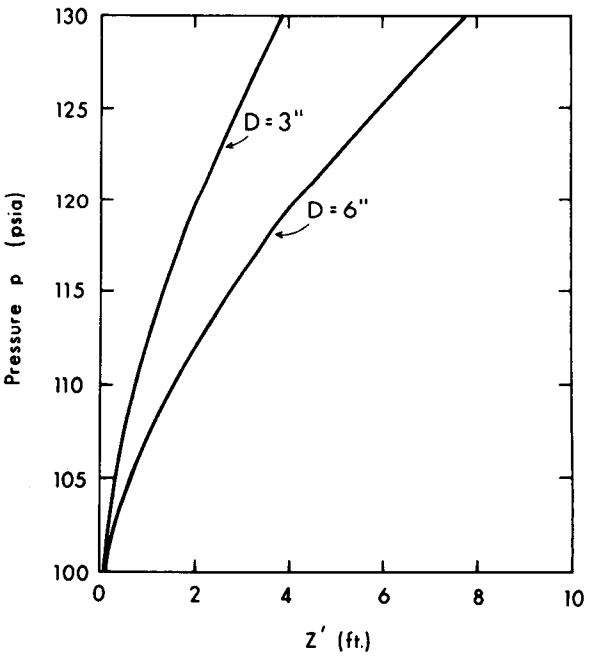

Fig. 30 Pressure Distribution in the Approach Region to Critical Flow with Lip Pressure at 100 psia